Giant Enhancement of Perpendicular Magnetic Anisotropy and Field-Free Switching Through Interfacial Engineering in Pt/Co/Pt Heterostructures

Yulin Zhang(张雨霖)[1†], Mingzhang Wei(卫鸣璋)[1†], Ziji Shao(邵子霁)[1†], Haodong Fan(樊浩东)[2†], Menghao Jin(金蒙豪)[1], Zhongshu Feng(冯重舒)[1], Xiaofeng Han(韩晓锋)[1], Changqiu Yu(于长秋)[1], Jiahong Wen(温嘉红)[1], Xinyu Shu(舒新愉)[1], and Tiejun Zhou(周铁军)[1,2,*]

[1]*School of Electronics and Information Engineering, Hangzhou Dianzi University, Hangzhou 310018, China*
[2]*State Key Laboratory of Spintronic Devices and Technologies, Hangzhou 311305, China*

(Received 9 October 2025; accepted manuscript online 7 January 2026)

The enhancement of perpendicular magnetic anisotropy (PMA) is critical for the continuous growth of magnetic memory density. Material systems that possess high interfacial PMA typically involve strong spin-orbit coupling (SOC) or transition metal/oxide interfaces. In contrast, the role of 3d light metals in enhancing the interfacial PMA has been less investigated. This study demonstrated that the insertion of a few atomic Cr layers into Pt/Co/Pt/Ta heterostructures with Cr between the 1 atomic Pt layer and the 3 nm Ta overlayer enhanced the effective PMA energy ($K_{\rm eff}$) by a factor of 4. First-principles calculations revealed that the underlying mechanism originated from Cr-Pt d-orbital hybridization, leading to a corresponding orbital redistribution and significantly increasing the magnetic anisotropy energy. The progressive reduction in the spin-orbit torque (SOT) efficiency with increasing Cr thickness might stem from the enhanced orbital Rashba–Edelstein effect at the Pt/Cr interface. Furthermore, the wedging of a few atomic Cr layers caused the robust field-free SOT switching of perpendicular magnetization, which was due to the lateral PMA gradients enabled by the strong dependence of the PMA on the Cr thickness. The results provide a method for interfacial PMA enhancement by d-orbital hybridization of 3d–5d electrons and an alternative to field-free SOT switching towards low-power and high-density memory applications.

DOI: 10.1088/0256-307X/43/3/030701 CSTR: 32039.14.0256-307X.43.3.030701

1. Introduction. Magnetic random access memory (MRAM) is a leading-edge storage technology that combines nonvolatility, low power consumption, high-speed operation, and excellent process compatibility.[1] Among its variants, the spin-orbit torque MRAM (SOT-MRAM) utilizes current-induced spin-orbit torque (SOT) to enable angular momentum transfer from the crystal lattice to the magnetic layer,[2–5] thereby achieving fast and low-power magnetic switching.[6–9] Ferromagnetic multilayers exhibiting perpendicular magnetic anisotropy (PMA), which are crucial for high-density memories, are key components of such devices.[10,11] Physically, PMA in bulk systems such as $L1_0$ FePt[12] and MnAl,[13–15] primarily stems from the uniaxial crystal field induced by the elongation or compression of the c-axis in the $L1_0$ crystal lattice.[16] Nevertheless, such materials typically require precise composition control, single-crystal substrates, or sophisticated seed-layer engineering, which restricts their application in SOT-MRAM.[16]

Unlike bulk PMA materials, interfacial PMA is suitable for extending the device compatibility to amorphous and polycrystalline systems. At ferromagnetic/oxide interfaces[17] (e.g., CoFeB/MgO, Co/Al_2O_3, and Co/MgO), PMA originates from the hybridization between the 3d orbitals of the ferromagnetic metal and O-2p orbitals. This hybridization causes symmetry breaking, leading to orbital redistribution along the z-axis and the emergence of a finite orbital moment $\langle L_z \rangle$, which in turn produces strong interfacial anisotropy. However, in ferromagnetic multilayers such as Co/Pt,[18–20] Co/Pd,[21,22] Co/Ni,[23,24] and Co/Cu,[25] interfacial orbital hybridization and strong spin–orbit coupling (SOC) enhance spin-orbit interactions, resulting in nonzero L_z. Specifically, in Co/Pt systems, SOC is critical for PMA generation and is largely influenced by the Z^4 scaling of the Bohr radius. The notable advantages in nonepitaxial integration possessed by such interfacial PMA systems make them suitable as pinning or free layers in magnetic tunnel junctions.[26]

In contrast, light elements, such as the 3d transition metal chromium (Cr), typically exhibit weak SOC and quenched orbital moments. Inserting a relatively thicker Cr layer of more than 1 nm in Pt/Co/Cr stacks with Cr in direct contact with Co slightly enhances the PMA.[27,28] Nevertheless, a Cr layer thicker than 1 nm is sufficient to suppress pure interfacial effects.[28] Owing to the rich physics and magnetism at the interfaces, interfacial engineering through one or a few atomic layers of Cr in

†These authors contributed equally to this work.
*Corresponding author. Email: tjzhou@hdu.edu.cn
© 2026 Chinese Physical Society and IOP Publishing Ltd. All rights, including for text and data mining, AI training, and similar technologies, are reserved.

Pt/Co/Pt heterostructures with Co and Cr layers bridged by approximately one atomic Pt layer might be able to restore the orbital moment and/or the magnetism of Cr at the interface, thereby enabling the possible enhancement of both magnetic anisotropy and magnetization.[29] Furthermore, such an enhancement could modify the SOT, leading to a change in the SOT efficiency and even field-free switching of the perpendicular magnetization, which warrants further investigation for high-density and low-power magnetic memories.

In this study, the insertion of a few atomic Cr layers into Pt/Co/Pt heterostructures with Co and Cr layers bridged by approximately one atomic Pt layer effectively modulated the effective PMA energy density $K_{\rm eff}$. The insertion of approximately three atomic Cr layers enhanced the PMA field and $K_{\rm eff}$ by factors of two and four, respectively. A combination of first-principles calculations and experimental measurements indicated that the enhancement originated from interfacial orbital hybridization at the Pt/Cr interface. The emergence of ferromagnetism at the interfacial Pt/Cr layer provided clear evidence of orbital redistribution, which together with ferromagnetic coupling to Co increased the total magnetic moment. The decrease in the SOT efficiency with increasing Cr thickness can be ascribed to the enhanced orbital Rashba–Edelstein effect (OREE) at the Pt/Cr interface. Finally, deterministic field-free magnetization switching was demonstrated using a wedged Cr layer to introduce lateral anisotropy gradients. These findings clarify the underlying physics of PMA enhancement by d-orbital hybridization of 3d–5d electrons, thereby broadening the material platforms with interfacial PMA, and offer a method for field-free SOT switching towards low-power and high-density memory applications.

2. Results and Discussions.

2.1. Magnetic Characterization. The magnetic multilayer structures of Ta/Pt/Co/Pt/Cr/Ta with varied Co thicknesses ($t_{\rm Co}$) and Cr thicknesses ($t_{\rm Cr}$) [Fig. 1(a)] were deposited onto Si/SiO_2 substrates by magnetron sputtering at room temperature, under a base pressure below 8×10^{-8} Torr (all thicknesses are in nanometers). A 0.25-nm thick Pt layer (approximately one atomic monolayer) was inserted between the Cr and Co. The magnetic properties were characterized using a superconducting quantum interference device. As typical examples, the hysteresis loops of the Ta(2)/Pt(3.5)/Co(0.7)/Pt(0.25)/Cr($t_{\rm Cr}$ = 0 and 0.5 nm)/Ta(3) stacks are shown in Fig. 1(b). The introduction of approximately three atomic layers of Cr (0.5 nm thick) between the Pt and Ta capping layers significantly increases both coercivity and saturation magnetization ($M_{\rm s}$). $M_{\rm s}$ almost doubles from 600 emu/cm^3 to approximately 1200 emu/cm^3, while the coercivity increases from approximately 10 Oe to approximately 180 Oe. Systematic measurements were performed on samples with various Co thicknesses ($t_{\rm Co}$) at $t_{\rm Cr}$ values of 0 and 0.5 nm, and the results are summarized in Fig. 1(c). These results reveal that the Cr layer consistently enhances $M_{\rm s}$ across the entire $t_{\rm Co}$ series possessing PMA. However, the increase decreases as the Co thickness increases, which aligns with this interfacial nature (see Figs. S1 and S2 in the Supplementary Material). Indeed, the experimentally observed dependence of the Cr-induced magnetization enhancement on the thickness of Co is consistent with this interfacial nature. Additionally, X-ray photoelectron spectroscopy analysis negated the possibility of Co oxidation

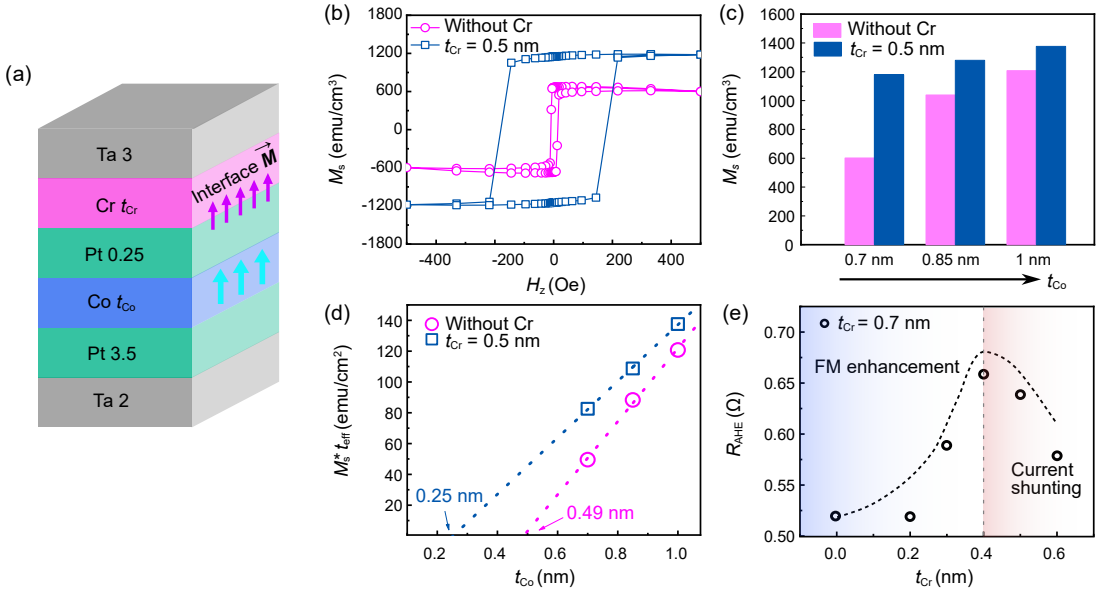

Fig. 1. Magnetic property measurements. (a) Schematic of PMA multilayer stack. The arrows at the bottom and top denote the magnetic moments of the Co layer and Pt/Cr interface, respectively. (b) Out-of-plane M–H loops and (d) linear fit of the magnetic dead-layer thickness of Ta(2)/Pt(3.5)/Co(0.7)/Pt(0.25)/Cr($t_{\rm Cr}$ = 0 or 0.5 nm)/Ta(3). (c) Saturation magnetization $M_{\rm s}$ as a function of various $t_{\rm Co}$ and $t_{\rm Cr}$. (e) Anomalous Hall resistence as a function of $t_{\rm Cr}$ when $t_{\rm Co}$ = 0.7 nm.

in the Ta(2)/Pt(3.5)/Co(0.7)/Ta(3) sample (Fig. S3). M_s is linearly fitted as a function of t_{Co} to extract the dead-layer thickness of Co (determined from the intercept on the t_{Co} axis), as shown in Fig. 1(d). The introduction of an insertion layer of Cr (0.5 nm) reduces the Co dead-layer thickness by 0.24 nm, corresponding to a 50% reduction compared to the Cr-free structure (which exhibits a 0.49-nm thick dead layer). These results collectively demonstrate that Cr insertion effectively suppresses the magnetic dead layer in the Pt/Co/Pt/Ta system, which partially contributes to the M_s increase.

The increased magnetic moment was further supported by the enhanced anomalous Hall resistance [Fig. 1(e)], which increased significantly with the insertion of one to a few atomic layers of Cr and peaked at $t_{Cr} = 0.4$ nm. This behavior could partially arise from the restored magnetic moment of Cr at the interface, that is, ferromagnetic Cr, which also enhanced the PMA, as evidenced by the significant increase in coercivity [Fig. 1(b)]. The decrease in Hall resistance beyond $t_{Cr} = 0.4$ nm is due to increased current shunting.

To clarify the mechanism underlying the enhancement of the magnetic moment and the perpendicular magnetic anisotropy, previous studies on capping layers in Pt/Co/X trilayer systems, where X typically represents an oxide or heavy metal, are considered. In oxide-capped structures, PMA originates from chemical bonding between oxygen ions and adjacent transition metal ions.[30,31] This chemical bonding involves the hybridization of oxygen sp orbitals with transition metal d_{z^2} orbitals, accompanied by a reduction in the degeneracy of the d-orbital. In contrast, heavy-metal capping layers enhance the PMA primarily through strong SOC.[29,32] Because surface ferromagnetism occurs in certain 3d transition metals,[33,34] the additional magnetic moment observed in our system can be attributed to the Cr layer.

2.2. PMA Characterization. Harmonic Hall voltage measurements were performed to systematically evaluate the enhancement of the PMA introduced by the ultrathin Cr insertion layer in the Pt/Co/Pt system. The PMA field (H_k) was determined from the first-harmonic Hall signal, as shown in Fig. S4 (see Supplementary Material, Note S3). The in-plane component of the magnetization, m_x, defined as $\sqrt{1-(m_z)^2}$, was obtained as a function of the in-plane magnetic field H_x. H_k was subsequently extracted by extrapolating the m_x–H_x relationship to the point at which $m_x = 1$.[34]

The extracted H_k values are plotted as a function of t_{Cr} in Fig. 2(a). H_k initially rises by nearly 60%, then continues to increase at a slower rate, and reaches a maximum of 1.392 T at $t_{Cr} = 0.5$ nm (approximately 3 atomic layers of Cr), which is almost double of that without Cr insertion (0.694 T). H_k was characterized by averaging the data from the three Hall bars to enhance the data rigor. Using the corresponding M_s values, the effective anisotropy energy density K_{eff} was calculated using $K_{eff} = H_K \cdot M_S/2$.[28,35] With the insertion of approximately three atomic Cr layers, K_{eff} increased sharply by 300% from 2.105 Merg/cm^3

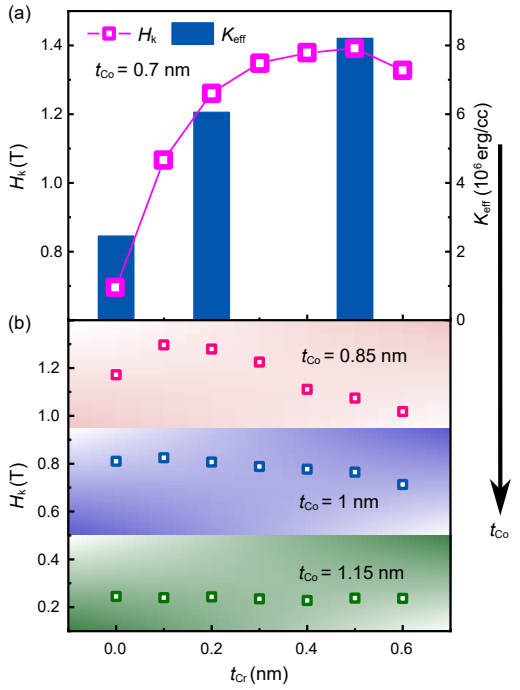

Fig. 2. Characterization of PMA in the Cr insertion layer. (a) Dependence of the PMA field (H_k) and effective anisotropy energy density (K_{eff}) on the Cr thickness (t_{Cr}) for the Ta(2)/Pt(3.5)/Co(0.7)/Pt(0.25)/Cr(t_{Cr})/Ta(3) stack. (b) Extracted H_k values as a function of t_{Cr} for various t_{Co}.

(without Cr) to 8.209 Merg/cm^3. Thus, Cr insertion substantially enhanced PMA in the Co/Pt system. In contrast, in the control samples lacking the Pt(0.25) spacer layer [Ta(2)/Pt(3.5)/Co(0.7)/Cr(t_{Cr})/Ta(3)], the PMA decreased slightly upon the insertion of an ultrathin Cr layer (Fig. S5). This stark contrast indicates that the ultrathin Cr/Co interface itself does not contribute to the strong PMA enhancement, which differs from the behavior observed at thicker Cr/Co interfaces. Instead, the presence of a thin Pt(0.25) layer at the interface is essential for the observed effect, indicating that the PMA enhancement primarily originates from interfacial orbital hybridization at the Pt/Cr interface (as confirmed by first-principles calculations below).

The Co-thickness-dependent effect was investigated by varying the, Co layer thicknesses. The measured H_k values are summarized in Fig. 2(b). The modulation effect of t_{Cr} on H_k weakens progressively with increasing Co layer thickness. Specifically, when Co = 0.85 nm, H_k first increases by 19% at a Cr insertion layer thickness of 0.1 nm and then gradually decreases as the thickness increases. When $t_{Co} = 1$ nm and 1.15 nm, the introduction of Cr produces a negligible change in H_k, indicating strong decay of the Cr-induced PMA enhancement. These findings highlight the pronounced interfacial-dominated PMA effect, which is more significant in thinner Co films. Thus, interfacial orbital hybridization is critical for the PMA mechanism, and its influence is confined to a limited region near the interface and diminishes as t_{Co} increases.[36,37]

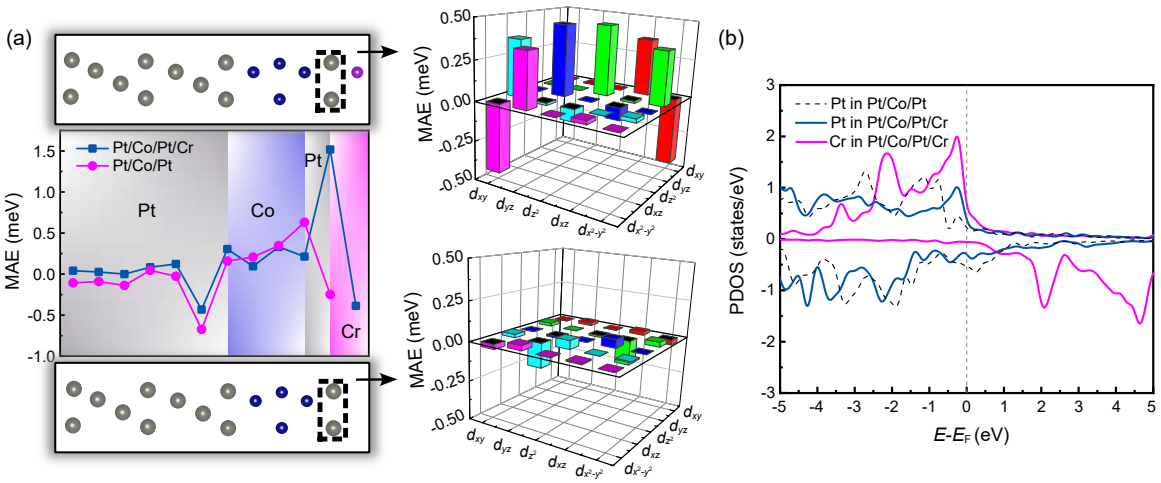

Fig. 3. (a) Layer-resolved MAE in Pt/Co/Pt (down) and Pt/Co/Pt/Cr heterostuctures (up). The black arrows indicate d-orbital resolved MAE of Pt/Co/Pt/Cr (up) and Pt/Co/Pt (down). (b) Projected density of states (PDOS) of the total d orbitals from interfacial Cr (pink) and Pt (dark green) in Pt/Co/Pt/Cr and Pt (dashed line) in Pt/Co/Pt.

2.3. First-Principles Calculations. To elucidate the mechanism underlying the enhanced interfacial PMA obtained by introducing Cr as a light 3d transition metal, first-principles calculations were performed. The total magnetic anisotropy energy (MAE) of the Pt/Co/Pt structure was calculated as 0.85 meV, which significantly increased to 2.14 meV with the introduction of Cr. Moreover, d-orbital resolved MAE analysis of the interfacial Pt layer was conducted Fig. 3(a). Modifications in the matrix elements $(d_{yz}, d_{x^2-y^2})$, (d_{xy}, d_{xz}), and (d_{yz}, d_{z^2}) with Cr contributed significantly to the PMA. According to second-order perturbation theory,[38] these orbital reconfigurations modulate spin-opposite orbital interactions. A decrease in these energetic gaps enhances the PMA contributions. Further analysis indicated that the d-orbital modifications of the interfacial Pt originated from Pt-Cr hybridization. As shown in Fig. 3(b), Cr induced a significant reconstruction of the occupied spin-up d orbital of Pt through hybridization. This interfacial electronic reconstruction induced the fundamental mechanism for PMA enhancement by ultrathin Cr. Furthermore, the theoretical results suggested that a few atomic Cr layers were ferromagnetically coupled with Co through the Pt layer, which partially contributed to M_s enhancement. In contrast, according to Bruno's model, which clearly links PMA and interfacial SOC,[39,40] PMA originates from the combined enhancement of interfacial SOC and the out-of-plane orbital magnetic moment. The 0.25 nm Pt interlayer in the proposed system enhanced the SOC at the Co/Pt interface, while the additional 3d–5d orbital hybridization at the Pt/Cr interface further increased the interfacial SOC strength. Together with the increased interfacial orbital moment, these effects significantly enhanced the PMA.

2.4. SOT Efficiency Characterization. Because the Cr insertion layer yielded the strongest PMA enhancement at $t_{Co} = 0.7$ nm, the SOT efficiency was systematically assessed using these samples. The damping-like effective field was determined using large-field second-harmonic measurements. When the in-plane magnetic field H_x exceeds H_k, $R_{2\omega}$ can be expressed by[41]

$$R_{2\omega} = \frac{1}{2}\frac{R_{AHE}H_{DL}}{|H_x| - H_k} + R_{offset}, \tag{1}$$

where H_{DL} and R_{offset} denote the damping-like effective field and offset resistance, respectively. A representative second-harmonic signal is shown in Fig. 4(a), with the dashed line corresponding to a nonlinear fit based on Eq. (1). As illustrated in Fig. 4(b), H_{DL} exhibits excellent linearity with respect to varying AC current amplitudes, which allows the damping-like field per unit current density ($\beta_{DL} = H_{DL}/J$) to be determined.

After accounting for the parallel current shunting model, β_{DL} decreased gradually with increasing t_{Cr} [Fig. 4(c)]. This trend differs from previous observations in Pt/Co/Cr systems,[28] where Pt, which possesses a spin Hall angle opposite in sign to that of the Cr layer (several nanometers thick), enhances the SOT efficiency. However, in the proposed structure, a one-atomic Pt layer is introduced between the Co and ultrathin Cr layers. Notably, Cr exhibits both high orbital Hall conductivity[42] and giant OREE at the interface, similar to that reported for the CuO_x/Pt system.[43] In the Pt(3.5 nm)/Co(0.7 nm)/Pt(0.25 nm)/Cr(0.1 nm–0.6 nm) stack, the primary mechanism for generating orbital current in the ultrathin Cr layer is the OREE at the Pt/Cr interface, where its inversion symmetry is broken.[44,45] Additionally, Co promotes orbital-spin conversion through $L \cdot S$ (orbital and spin angular momentum) coupling, particularly in Pt/Co systems with strong SOC.[46,47] When a charge current is applied, an interface orbital moment is generated and injected into the neighboring Co/Pt layer, where it is efficiently converted into a spin current. As the Cr layer thickness increases, this mechanism significantly affects SOT switching and SOT efficiency. Owing to the positive orbital spin conversion coefficient of Pt and the positive orbital Hall conductivity of Cr,[44] the Cr-induced spin current partially cancels

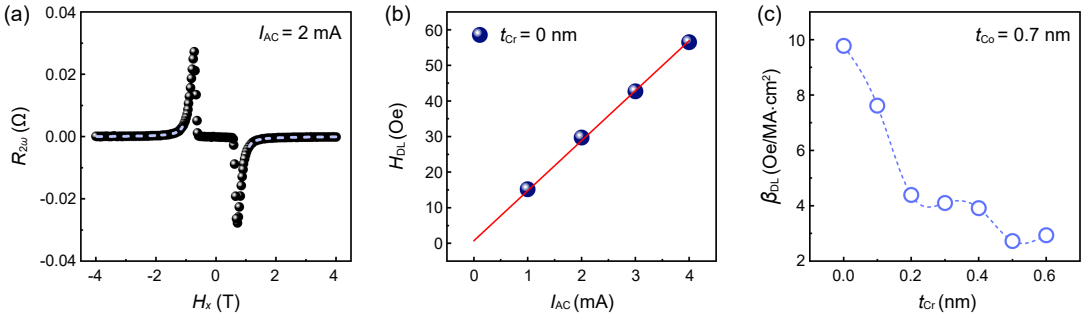

Fig. 4. SOT efficiency characterization. (a) Second harmonic resistance as a function of the in-plane magnetic field H_x under $I_{AC} = 2\,\text{mA}$, $t_{Cr} = 0\,\text{nm}$, and $t_{Co} = 0.7\,\text{nm}$. The nonlinear fits are shown as dashed lines. (b) Damping-like effective field H_{DL} versus AC current magnitude for $t_{Cr} = 0$ nm and $t_{Co} = 0.7\,\text{nm}$, where the linear fit is represented by the solid line. (c) Variation of the effective field per unit current density, β_{DL}, with t_{Cr} at $t_{Co} = 0.7\,\text{nm}$; the trend is indicated by the dashed line.

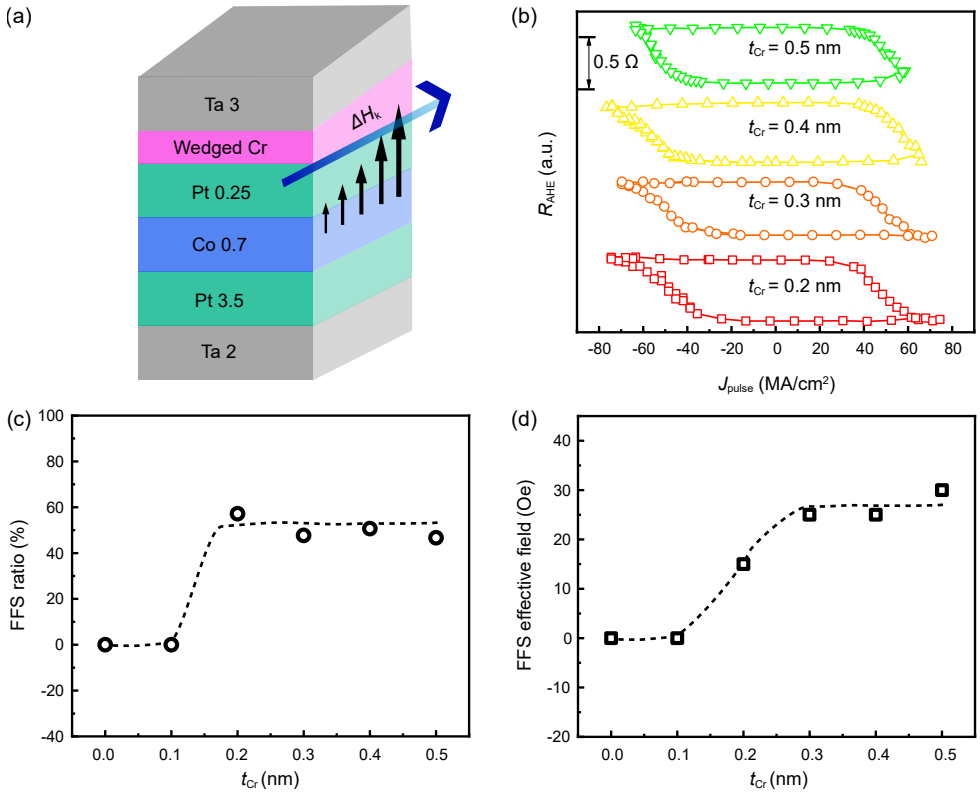

Fig. 5. Field-free SOT switching induced by a wedged Cr layer. (a) Schematic of the multilayer stack: Ta(2)/Pt(3.5)/Co(0.7)/Pt(0.25)/wedged Cr (with an average thickness of $\bar{t}_{Cr}$)/Ta(3). The blue arrow indicates the lateral anisotropy gradient (ΔH_k) generated by the thickness gradient of the Cr layer. (b) FFS behavior as a function of $\bar{t}_{Cr}$. (c) Corresponding FFS ratio and (d) FFS effective field plotted against $\bar{t}_{Cr}$.

the spin current generated by the spin Hall effect from the underlying Pt layer. Consequently, the overall SOT efficiency gradually declines with increasing Cr thickness. In addition, the SOT efficiency of the reference sample [Ta(2)/Pt(3.5)/Co(0.7)/Cr(t_{Cr})/Ta(3)] without Pt(0.25) increased slightly with the thickness of the ultrathin Cr layer (Fig. S6). The opposite trends in SOT efficiency with Cr thickness observed in the two sets of samples demonstrate the critical role of the Pt(0.25) layer and provide potential evidence for OREE at the Pt/Cr interface.

2.5. Field-Free Switching. Based on the effective modulation of the PMA by the ultrathin Cr insertion layer, a wedged Cr layer was introduced to enable current-induced SOT field-free switching (FFS), as schematically shown in Fig. 5(a). The wedged Cr layer (wedge along the y-direction) was fabricated by stopping the substrate rotation during deposition. A comparison of the H_k values of the wedged and flat samples showed minimal variation (Fig. S7). Furthermore, while deterministic switching in uniform (non-wedged) control samples required an external magnetic field, FFS in wedged samples was achieved only when the current was applied perpendicular to the wedge direction (e.g., along the x-direction), as shown in Fig. S8. Figure 5(b) shows that a distinct FFS is observed

when $\bar{t}_{Cr} \geq 0.2\,nm$. In contrast, no FFS is detected for the 0.1 nm-wedged Cr, as this thickness is below that of a single atomic layer. As t_{Cr} increases, the FFS ratio gradually increases and eventually approaches saturation, as shown in Fig. 5(c). To quantify the effective field required for FFS, SOT measurements were conducted under various in-plane magnetic fields (Fig. S9). The FFS effective field is defined as the in-plane field at which SOT switching vanishes. Its dependence on $\bar{t}_{Cr}$ followed a trend identical to that of the FFS ratio [Fig. 5(d)], confirming their close correlation.

The mechanism that enables FFS is distinct from conventional spin-source symmetry-breaking schemes because the wedged Cr layer does not break the symmetry of the underlying spin source. Rather, the effect is primarily caused by the lateral anisotropy gradient [48,49] introduced by the Cr wedge [Fig. 5(a)]. This gradient in H_k (ΔH_k), which directly results from its dependence on t_{Cr} [Fig. 2(a)], breaks the SOT symmetry and provides a deterministic energy preference for the FFS. Although a concomitant Dzyaloshinskii-Moriya interaction gradient may form owing to the varying Pt/Cr interface, its contribution should be considered secondary because of the strong correspondence between the switching behavior and H_k enhancement. Together, these findings emphasize the dual role of the ultrathin Cr layer in enhancing PMA and enabling FFS in Pt/Co heterostructures.

3. Conclusion. In summary, the insertion of a few atomic Cr layers resulted in pronounced enhancement and interfacial modulation of the PMA in Pt/Co/Pt heterostructures. At the optimal Cr thickness, H_k and K_{eff} were enhanced by factors of two and four, respectively. This enhancement was accompanied by a net increase in the magnetic moment owing to the restoration of ferromagnetism in the interfacial Cr layer and its ferromagnetic coupling with Co. First-principles calculations traced the origin of the increased MAE to the Cr-Pt d-orbital hybridization and provided direct evidence of interfacial orbital redistribution. The decrease in the SOT efficiency with increasing t_{Cr} was attributed to the enhanced orbital Rashba–Edelstein effect at the Pt/Cr interface. Moreover, field-free SOT switching was achieved by leveraging the lateral anisotropy gradient created by the wedged Cr layer. These findings underscore the potential of light 3d metals for PMA modulation via a mechanism distinct from conventional heavy-metal spin-orbit coupling or oxygen-mediated interfacial effects.

4. Method.

4.1. Sample Preparation and Characterization. All films were deposited by a magnetron sputtering system with a base pressure greater than 8×10^{-8} Torr. The Hall-bar structures were patterned into $10\,\mu m \times 10\,\mu m$ by laser direct writer and Ar ion milling. Electrical contacts were formed by a lift-off procedure using Cr (10 nm)/Cu (80 nm). The harmonic Hall voltage and current-induced SOT switching were measured in three-dimensional superconducting magnet using a Keithley 6221 and SR830 (Stanford Research Systems). The pulse width was set to 30 µs. The current shunting of each layer and the related resistivity were determined by subtracting the sheet conductance of Ta(2 nm)/Co(t_{Co})/Pt(0.25 nm)/Ta(3 nm) from the that of the entire stack Ta(2 nm)/Pt(3.5 nm)/Co(t_{Co})/Pt(0.5 nm)/Cr(t_{Cr})/Ta(3 nm). The M–H loops were acquired using MPMS-3 (Quantum Design).

4.2. Calculation Method. The ionic relaxations and electronic and magnetic properties were calculated in the framework of density functional theory [50] within the Perdew-Burke-Ernzerhof exchange-correlation functional [51] as implemented in the VASP package. [52] The projector-augmented wave approach [53–55] was used to describe ion-electron interactions. The valence electrons for Pt, Co, and Cr were chosen as $5d^9 6s^1$, $3d^8 4s^1$, and $3p^6 3d^5 4s^1$, respectively. The GGA+U method [56] was used with an effective U_{eff} of 2 eV for the 3d orbitals of the Cr atoms. [57] The plane-wave cutoff energy was set to 520 eV. The first Brillouin zone was sampled using Monkhorst–Pack k mesh grids of $16 \times 16 \times 16$ and $24 \times 24 \times 24$ for structure optimization and property calculations, respectively. The MAE was obtained by calculating the energy difference delta between the in-plane [100] and out-of-plane [001] magnetization orientations, considering the spin-orbit interaction. The positive and negative MAE values correspond to the PMA and in-plane magnetic anisotropy, respectively.

Acknowledgments. This work was supported by the "Pioneer" and "Leading Goose" R&D Program of Zhejiang Province (Grant No. 2022C01053), the National Natural Science Foundation of China (Grant No. 62293493), and the Natural Science Foundation of Zhejiang Province, China (Grant No. LQ21A050001). Moreover, we thank Zhan-er He from Instrumentation and Service Center for Physical Sciences at Westlake University for their extensive assistance in SQUID-VSM measurements.

References

[1] Nguyen V D, Rao S, Wostyn K, and Couet S 2024 *npj Spintronics* **2** 48
[2] Manchon A, Železný J, Miron I M, Jungwirth T, Sinova J, Thiaville A, Garello K, and Gambardella P 2019 *Rev. Mod. Phys.* **91** 035004
[3] Zhu L J 2023 *Adv. Mater.* **35** 2300853
[4] Song C, Zhang R Q, Liao L Y, Zhou Y J, Zhou X F, Chen R Y, You Y F, Chen X Z, and Pan F 2021 *Prog. Mater. Sci.* **118** 100761
[5] Han X F, Wang X, Wan C H, Yu G Q, and Lv X R 2021 *Appl. Phys. Lett.* **118** 120502
[6] Fukami S, Zhang C L, DuttaGupta S, Kurenkov A, and Ohno H 2016 *Nat. Mater.* **15** 535
[7] Fan H D, Shao Z J, Wang J L, Jin M H, Wu B R, Feng Z S, Wei M Z, Yu C Q, Wen J H, Li H, Chen T W, Liu B, Li W J, and Zhou T J 2023 *Phys. Rev. B* **108** 224409
[8] Lau Y C, Betto D, Rode K, Coey J M D, and Stamenov P 2016 *Nat. Nanotechnol.* **11** 758
[9] Fan H D, Jin M H, Wu B R, Wei M Z, Wang J L, Shao Z J, Yu C Q, Wen J H, Li H, Li W J, and Zhou T J 2023 *Appl. Phys. Lett.* **122** 262404

[10] Oh Y W, Baek S H C, Kim Y M, Lee H Y, Lee K D, Yang C G, Park E S, Lee K S, Kim K W, Go G, Jeong J R, Min B C, Lee H W, Lee K J, and Park B G 2016 *Nat. Nanotechnol.* **11** 878

[11] Fan H D, Jin M H, Luo Y M, Yang H X, Wu B R, Feng Z S, Zhuang Y S, Shao Z J, Yu C Q, Li H, Wen J H, Wang N N, Liu B, Li W J, and Zhou T J 2023 *Adv. Funct. Mater.* **33** 2211953

[12] Wang H, Rahman M T, Zhao H B, Isowaki Y, Kamata Y, Kikitsu A, and Wang J P 2011 *J. Appl. Phys.* **109** 07B754

[13] Nie S H, Zhu L J, Lu J, Pan D, Wang H L, Yu X Z, Xiao J X, and Zhao J H 2013 *Appl. Phys. Lett.* **102** 152405

[14] Sun H L, Zhao X P, Han R K, Zhang C, Liu L, Qin H R, Xie Z C, Deng H X, Pan D, and Wei D H 2024 *Appl. Phys. Lett.* **124** 102404

[15] Sun H L, Han R K, Qin H R, Zhao X P, Xie Z C, Wei D H, and Zhao J H 2024 *Chin. Phys. Lett.* **41** 057503

[16] Tudu B and Tiwari A 2017 *Vacuum* **146** 329

[17] Oh Y W, Lee K D, Jeong J R, and Park B G 2014 *J. Appl. Phys.* **115** 17C724

[18] Harp G, Weiler D, Rabedeau T, Farrow R, and Marks R 1993 *MRS Online Proceedings Library* **313** 493

[19] Victora R H and MacLaren J M 1993 *J. Appl. Phys.* **73** 6415

[20] Yan Z, Li Z, Zhu L, Lin X, and Zhu L 2025 *Chin. Phys. Lett.* **42** 090701

[21] Purcell S T, Johnson M T, McGee N W E, De Vries J J, Zeper W B, and Hoving W 1993 *J. Appl. Phys.* **73** 1360

[22] Engel B N, England C D, Van Leeuwen R A, Wiedmann M H, and Falco C M 1991 *Phys. Rev. Lett.* **67** 1910

[23] Johnson M, De Vries J, McGee N, Aan de Stegge J, and Den Broeder F 1992 *Phys. Rev. Lett.* **69** 3575

[24] Daalderop G, Kelly P, and Den Broeder F 1992 *Phys. Rev. Lett.* **68** 682

[25] Hillebrands B, Krams P, Fassbender J, Mathieu C, Güntherodt G, Jungblut R, and Johnson M T 1994 *Acta. Phys. Pol. A* **85** 179

[26] Nguyen V D, Talmelli G, Monteiro M G, Palomino A, Kateel V, Giuliano D, Van Beek S, Vander Meeren N, Vergel N F, and Wostyn K 2024 *IEEE International Electron Devices Meeting (IEDM)* 1

[27] Cui B S, Chen S W, Li D, Yun J J, Guo X B, Wu K, Zhang X, Wang Y P, Zuo Y L, and Gao M Z 2017 *Appl. Phys. Express* **11** 013001

[28] Cui B S, Yun J J, Yang K Y, Wu H, Zhu Z D, Zuo Y L, Yang D Z, Gao M Z, Zhang Z Z, and Xi L 2019 *Appl. Phys. Express* **12** 043001

[29] Ueno T, Sinha J, Inami N, Takeichi Y, Mitani S, Ono K, and Hayashi M 2015 *Sci. Rep.* **5** 14858

[30] Manchon A, Ducruet C, Lombard L, Auffret S, Rodmacq B, Dieny B, Pizzini S, Vogel J, Uhlíř V, and Hochstrasser M 2008 *J. Appl. Phys.* **104** 043914

[31] Rodmacq B, Manchon A, Ducruet C, Auffret S, and Dieny B 2009 *Phys. Rev. B* **79** 024423

[32] Zhang B Y, Cao A N, Qiao J F, Tang M H, Cao K H, Zhao X X, Eimer S, Si Z Z, Lei N, and Wang Z H 2017 *Appl. Phys. Lett.* **110** 012405

[33] Fu C and Freeman A J 1986 *Phys. Rev. B* **33** 1755

[34] Guo Q X, Wang K, Bai H, Zheng Z C, Wang L H, Wang X M, He W, Yu G H, Teng J, and Zhu T 2022 *Appl. Phys. Lett.* **120** 022402

[35] Zhou B, Khanal P, Benally O J, Lyu D, Gopman D B, Enriquez A, Habiboglu A, Warrilow K, Wang J P, and Wang W G 2023 *Sci. Rep.* **13** 3454

[36] Parkin S, More N, and Roche K 1990 *Phys. Rev. Lett.* **64** 2304

[37] Du C H, Wang H L, Yang F Y, and Hammel P C 2014 *Phys. Rev. B* **90** 140407

[38] Wang D S, Wu R Q, and Freeman A J 1993 *Phys. Rev. B* **47** 14932

[39] Zhu L J, Zhu L J, Ma X, Li X Q, and Buhrman R A 2022 *Commun. Phys.* **5** 151

[40] Zhu L J, Lujan D, and Li X Q 2024 *Sci. China Phys. Mech.* **67** 227511

[41] Wu H, Xu Y, Deng P, Pan Q, Razavi S A, Wong K, Huang L, Dai B, Shao Q, Yu G, Han X, Rojas-Sanchez J C, Mangin S, and Wang K L 2019 *Adv. Mater.* **31** 1901681

[42] Jo D, Go D, and Lee H W 2018 *Phys. Rev. B* **98** 214405

[43] Ding S, Ross A, Go D, Baldrati L, Ren Z, Freimuth F, Becker S, Kammerbauer F, Yang J, and Jakob G 2020 *Phys. Rev. Lett.* **125** 177201

[44] Lee S, Kang M G, Go D, Kim D, Kang J H, Lee T, Lee G H, Kang J, Lee N J, and Mokrousov Y 2021 *Commun. Phys.* **4** 234

[45] Xie H, Zhang N, Ma Y T, Chen X, Ke L, and Wu Y H 2023 *Nano Lett.* **23** 10274

[46] Yang Y, Wang P, Chen J, Zhang D, Pan C, Hu S, Wang T, Yue W, Chen C, and Jiang W 2024 *Nat. Commun.* **15** 8645

[47] Lee D, Go D, Park H J, Jeong W, Ko H W, Yun D, Jo D, Lee S, Go G, and Oh J H 2021 *Nat. Commun.* **12** 6710

[48] Yu G Q, Upadhyaya P, Fan Y B, Alzate J G, Jiang W J, Wong K L, Takei S, Bender S A, Chang L T, Jiang Y, Lang M R, Tang J S, Wang Y, Tserkovnyak Y, Amiri P K, and Wang K L 2014 *Nat. Nanotechnol.* **9** 548

[49] Wu H, Nance J, Razavi S A, Lujan D, Dai B Q, Liu Y X, He H R, Cui B S, Wu D, Wong K, Sobotkiewich K, Li X Q, Carman G P, and Wang K L 2021 *Nano Lett.* **21** 515

[50] Kohn W and Sham L J 1965 *Phys. Rev.* **140** A1133

[51] Perdew J P, Burke K, and Ernzerhof M 1996 *Phys. Rev. Lett.* **77** 3865

[52] Kresse G and Furthmüller J 1996 *Phys. Rev. B* **54** 11169

[53] Kresse G and Hafner J 1993 *Phys. Rev. B* **47** 558

[54] Kresse G and Hafner J 1994 *Phys. Rev. B* **49** 14251

[55] Kresse G and Furthmüller J 1996 *Comp. Mater. Sci.* **6** 15

[56] Anisimov V I, Aryasetiawan F, and Lichtenstein A I 1997 *J. Phys.: Condens. Matter* **9** 767

[57] Cui Q R, Liang J H, Shao Z J, Cui P, and Yang H X 2020 *Phys. Rev. B* **102** 094425